processes

MDPI

Article

Coarse X-ray Lumbar Vertebrae Pose Localization and Registration Using Triangulation Correspondence

Watcharaphong Yookwan [1], Sornsupha Limchareon [2], Sang-Hun Lee [3], Jun-Su Jang [3], Daesung Lee [4,*] and Krisana Chinnasarn [1,*]

[1] Faculty of Informatics, Burapha University, Chon Buri 20131, Thailand
[2] Faculty of Medicine, Burapha University, Chon Buri 20131, Thailand
[3] Korea Institute of Oriental Medicine Daejeon, Daejeon 34054, Republic of Korea
[4] Department of Computer Engineering, Catholic University of Pusan, Busan 46265, Republic of Korea
* Correspondence: dslee@cup.ac.kr (D.L.); krisana@buu.ac.th (K.C.)

Abstract: Plain film X-ray scanners are indispensable for medical diagnostics and clinical procedures. This type of device typically produces two radiographic images of the human spine, including the anteroposterior and lateral views. However, these two photographs presented perspectives that were distinct. The proposed procedure consists of three fundamental steps. For automated cropping, the grayscale lumbar input image was initially projected vertically using its vertical pattern. Then, Delaunay triangulation was performed with the SURF features serving as the triangle nodes. The posture area of the vertebrae was calculated by utilizing the edge density of each node. The proposed method provided an automated estimation of the position of the human lumbar vertebrae, thereby decreasing the radiologist's workload, computing time, and complexity in a variety of bone-clinical applications. Numerous applications can be supported by the results of the proposed method, including the segmentation of lumbar vertebrae pose, bone mineral density examination, and vertebral pose deformation. The proposed method can estimate the vertebral position with an accuracy of 80.32 percent, a recall rate of 85.37 percent, a precision rate of 82.36%, and a false-negative rate of 15.42 percent.

Keywords: X-ray; vertebrae pose localization; Delaunay triangulation; SURF features

Citation: Yookwan, W.; Limchareon, S.; Lee, S.-H.; Jang, J.-S.; Lee, D.; Chinnasarn, K. Coarse X-ray Lumbar Vertebrae Pose Localization and Registration Using Triangulation Correspondence. *Processes* **2023**, *11*, 61. https://doi.org/10.3390/pr11010061

Academic Editors: Jun-Ho Huh and Yeong-Seok Seo

Received: 31 October 2022
Revised: 1 December 2022
Accepted: 22 December 2022
Published: 27 December 2022

1. Introduction

Digital image segmentation automates or simplifies the delineation of anatomical features and other regions of interest in a wide range of medical imaging applications [1–6]. Image segmentation is utilized in a variety of medical applications to classify the unique anatomical elements, such as the vertebrae, bones, and soft problems. Due to the great degree of resemblance across images of the same biological class, it is necessary to discern the low-level image properties of the item of interest, such as the form of the vertebra body in the case of spine images, in order to establish an accurate medical diagnosis. The indexing of medical images is another possible application of this information. The majority of segmentation research in medical imaging has focused on magnetic resonance (MR) [7–11] or computed tomography (CT) [12–16] images. Significantly less study and development have been devoted to the segmentation of X-ray pictures. In this study, we provide an X-ray-applicable methodology for investigating the vertebral mobility. The framework is based solely on the recognition of faces and the corner vertebrae, a revolutionary technique. We intend to create a computer vision application for use with the X-ray images of medical patients that will evaluate the vertebral movement and compare the mobility of each vertebra to that of other vertebrae in the same image. In today's environment, the study of the biomechanical changes in the spinal column is especially crucial because they are thought to be the primary cause of back pain. A tool used to assess the spinal column globally is called vertebral metrics. This image processing-based method

enables the identification of the X, Y, and Z positions of each spinal process in the standing position non-invasively and semi-automatically [17,18].

Traditional picture segmentation techniques assume that the regions to be segmented have uniform properties. According to this notion, segmentation. The input images are divided into areas based on the homogeneity of the requirements for the feature extraction [19,20]. Unfortunately, these homogeneity requirements cannot be satisfied for large and intricate X-ray images. Therefore, the segmentation of X-ray images of the spine is often performed using a hierarchical approach. The distinct area of the image, comprising the primary spine region, is initially segmented with a low degree of precision. The spine is then separated into the vertebrae [21,22]. Border detection is yet another way. Moreover, there are research projects that address this issue, but they have failed. Numerous studies have developed segmentation strategies for the vertebrae utilizing MRI imaging. Disc diagnosis in clinical lumbar MRI scans was automated using machine learning and heuristics in [23–28]. HOG and SVM are utilized as classifiers in this study. Many clinical cases were discovered with a 99 percent accuracy. Using the GVF snake, a method for segmenting the location of the vertebrae was presented. This work developed a semi-automatic segmentation technique in which the region of interest was manually annotated prior to its automatic retrieval. In the fields of graphics and computer vision, research on the three-dimensional (3D) representations produced by computational systems is both active and ongoing, making realistic human models in 3D poses [29–31], and 3D models of an organ.

According to the low contrast and noisy properties of an X-ray image, the mentioned state-of-the-art method failed to achieve the segmentation task. To raise the precision and decrease the number of errors in the exceedingly challenging human spinal segmentation procedure, an algorithm for finding the vertebrae pose area is presented.

- To pinpoint the posture area of the lumbar vertebrae in environments with a low contrast. Figure 1 depicts the position of the vertebrae that must be located. Thus, each stance is observed to be difficult to execute.

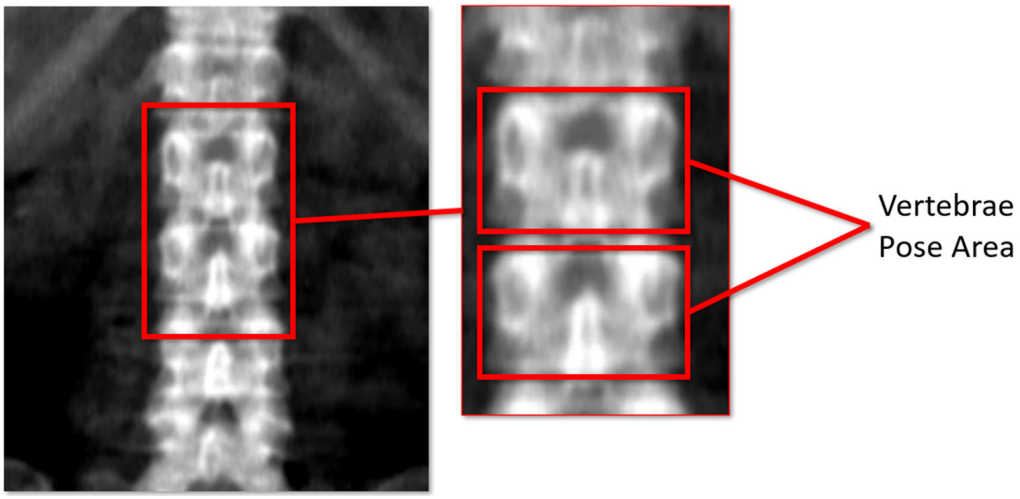

Figure 1. Lumbar vertebrae pose in low contrast condition.

- To register two sides of view for reconstructing a three-dimensional model.

The remaining sections of this article are structured as follows: Section 2 provides context for this research, and the region of interest segmentation, SURF. The extraction of the features, the creation of a triangle mesh using Delaunay triangulation, and the localization of the vertebrae pose region. Section 3, the Experimental Results and Discussion, and Section 4 is the Conclusions of this research are displayed.

2. Materials and Methods

2.1. Materials

2.1.1. X-ray Image of Human Lumbar Spine

Compared to CT and MRI, lumbar spine planar X-rays are of little diagnostic utility. However, fluoroscopy makes use of the talent, and much of the learned information and practice may be used for understanding more sophisticated imaging. Because of the transparency of the bones, which causes the overlapping of the features, especially in the anteroposterior view, an interpretation might be difficult.

The lumbar spine extends from below the twelfth and last thoracic vertebra (T12) to the top of the sacral spine, also known as the sacrum (S1) [8]. The majority of people have five lumbar vertebrae (L1–L5), although it is not unheard of to have six. The levels of the lumbar spine are numbered, beginning with L1 and ending with L5 or L6. The structure of human spine is demonstrated in Figure 2.

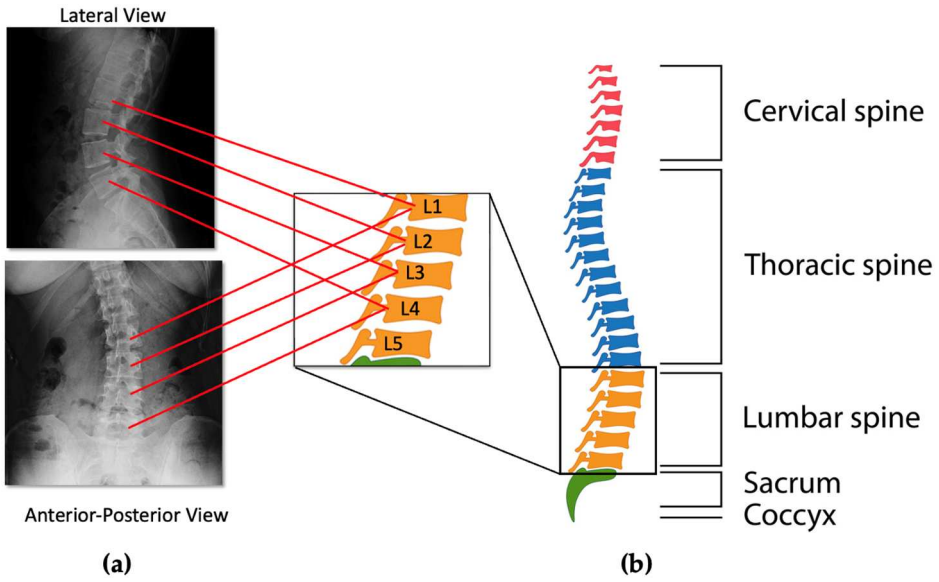

Figure 2. X-ray image of lumbar (**a**) and structure of human spine (**b**).

2.1.2. Speeded up Robust Features (SURF)

SURF is an acronym for the patented local feature detector and descriptor known as the speeded up robust features [9] in the field of computer vision. Possible applications include object detection, image registration, categorization, and even three-dimensional model reconstruction. This descriptor was partially influenced by the SIFT (scale-invariant feature transform) descriptor. The initial version of the SURF is considerably faster than SIFT, and SURF's designers believe it is more resilient than SIFT at managing varied image alterations.

SURF employs an integer approximation of the determinant of the Hessian blob detector to locate the regions of interest. Using three integer operations and a previously computed integral image, this determinant can be calculated. Its feature descriptor is calculated using the entire Haar wavelet response from the region surrounding the point of interest. Using the integral image, they can also be computed. The use of SURF descriptors has allowed for the localization and recognition of the items, persons, and faces, as well as the reconstruction of three-dimensional scenes, the tracking of objects, and the extraction of places of interest.

2.1.3. Delaunay Triangulation

A Delaunay triangulation, commonly referred to as a Delone triangulation, is a type of triangulation in mathematics and computational geometry. It is defined as a triangulation DT(P) for a set P of discrete points at a generic location, constructed so that no point

in P sits within the circumcircle of any triangle in DT (P). Because they optimize the minimum of all of the angles of the contained triangles, Delaunay triangulations prefer to avoid sliver triangles. Figure 3 illustrates the example Delaunay triangulation; the red point and red edge represent an image's features. The black point shows the network of Delaunay triangulation.

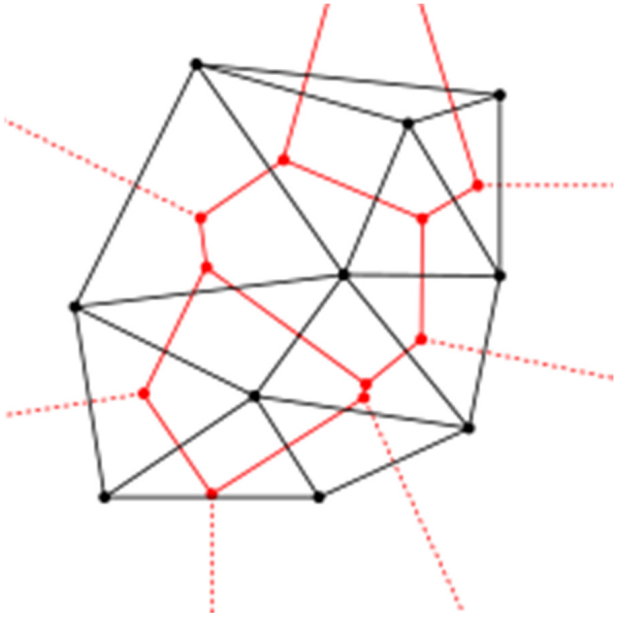

Figure 3. Visualization of Delaunay triangulation.

2.1.4. Dataset

The 3600 entries in the BUU-LSPINE dataset are X-rays of the lumbar spine (7200 images). Figure 4 depicts record includes the anteroposterior (AP view) and lateral (LA view) perspectives of the X-ray image. Each image includes the first sacral base and all five lumbar vertebrae (Lumbar: L1–L5) (Sacrum: S1). Patients are shown to be looking to the left in the LA view photographs. As a basis for each photograph, annotated CSV files are provided.

Figure 4. X-ray images in AP view (**a**) and Lateral view (**b**).

The patient's body part is the "LSPINE" (lumbar spine). The details of the dataset BUU-LSPINE are described in Table 1.

Table 1. Description of the experimented dataset which collected from Burapha University Hospital, Thailand.

	List	Description	Unit
1.	Image type	Normal X-ray (Plain film)	-
2.	Body part	Lumbar spine (LSPINE)	-
3.	View	AP view and LA view	-
4.	Numbers of patients	3600	records
5.	Numbers of images	7200	images
6.	Numbers of disorder patient	621	records
7.	Numbers of spinal disorders	788	cases
8.	Dataset size	18.5	GB
9.	Ground truth	1. Lumbar vertebrae positions. 2. Spondylolisthesis diagnosis. 3. Bertolotti's syndrome	-
10.	Ground truth type	Four corner coordinates points.	-
11.	File types	JPG (image) and CSV (ground truth)	-
12.	Locations	Thailand, Chonburi, Burapha University Hospital (BUH)	-
13.	Years of records	2000–2021	-
14.	Age range	(6–97)	years old
15.	Image dimension	Original	-
16.	Motivation	Delivering gold standard lumbar spine dataset of Thais for researchers around the world to develop and improve performance of the segmentation algorithms on the lumbar spine.	-

2.2. Methodology

The suggested algorithm involves three primary steps. Initially, the grayscale input lumbar image was projected vertically using its vertical pattern for automatic cropping. Using its SURF features as triangle nodes, Delaunay triangulation was then carried out. Finally, the vertebral posture area was estimated by calculating the edge density of the nodes. The briefed description is illustrated in Figure 5.

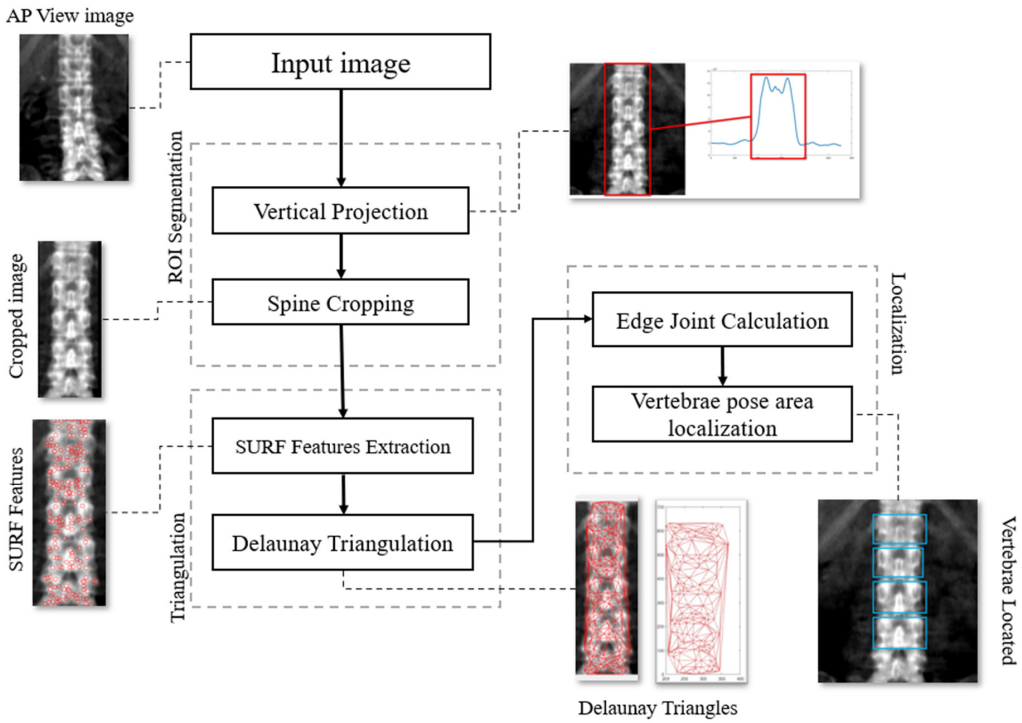

Figure 5. Outline of proposed framework.

2.2.1. Region of Interest Segmentation (ROI)

For eliminating the outer area of the X-ray image, the coarsely determination of the spine area is performed using vertical projection as in Figure 6. To project the grayscale image, the vertical projection can be expressed as Equation (1):

$$H_k(X) = \sum_{i=1}^{n} X_{k,i} \tag{1}$$

where $H_k(X)$ is a vertical projection of each k column of the image, n is the whole number of columns, and i is a number of the image's row of each k

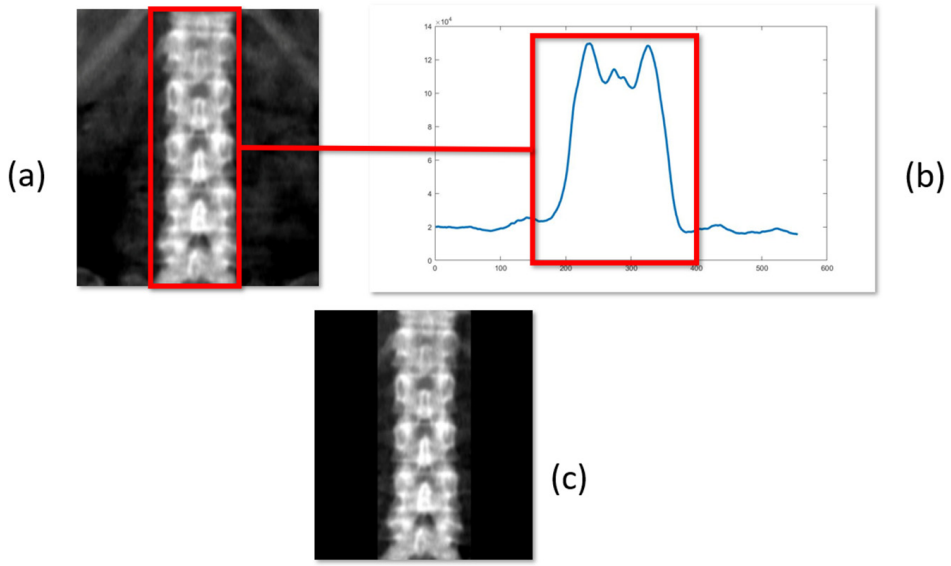

Figure 6. Original Input image (**a**) vertical projection graph (**b**) and result of spine cropping (**c**).

After applying a vertical projection profile to an image, a normal distribution pattern can be observed in the data. The normal distribution equation is applied to calculate the ROI (region of interest) from the graph. Using normal distribution, the image is then correctly cropped.

2.2.2. Triangulation Using Delaunay's Approach

To generate the Delaunay triangulation mesh, Figure 7 extracts the most relevant features from the cropped image to serve as the nodes (a). The detector is responsible for locating the interest points in an image, while the descriptor is accountable for identifying the features of the interest points and constructing the feature vectors corresponding to the interest points. The SURF properties are unaffected by the translation, rotation, or scaling transformations, but are marginally affected by the illumination and affine transformations as shows in Equation (2).

$$H(x,\sigma) = \begin{pmatrix} L_{xx}(X,\sigma) & L_{xy}(X,\sigma) \\ L_{xy}(X,\sigma) & L_{yy}(X,\sigma) \end{pmatrix} \tag{2}$$

where $L_{xx}(X,\sigma)$ is the convolution of the Gaussian second order derivative $\frac{\partial^2}{\partial x^2} g(\sigma)$ with the image I in point x, and similarly for $L_{xy}(X,\sigma)$ and $L_{yy}(X,\sigma)$.

The nodes determined by the SURF features then triangulated using Delaunay triangulation as shown in Figure 7b. This procedure's result structure is utilized during the localization stage. The Delaunay triangulation can be formulated in Algorithm 1.

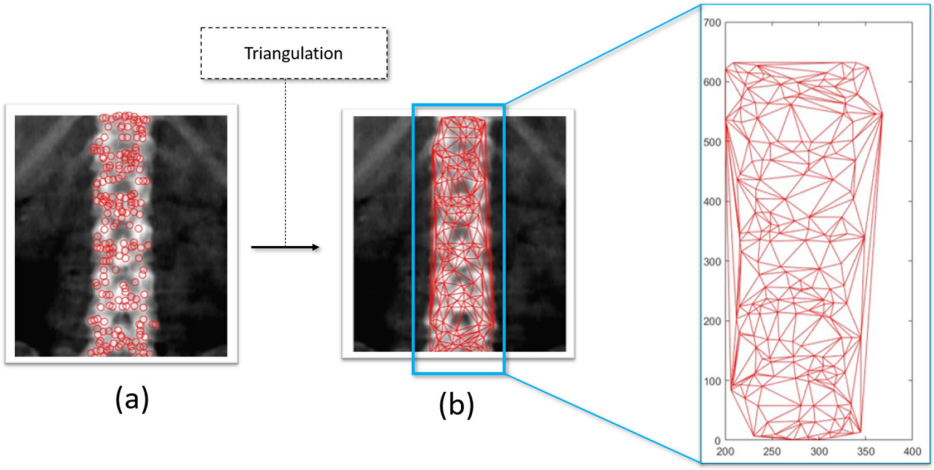

Figure 7. (**a**) SURF features plot and (**b**) Delaunay triangulation.

Algorithm 1 Delaunay triangulation

Algorithm Delaunay(P)
Input a set P of n point in $\mathbb{R}^2$
Output $\mathcal{DT}(P)$

1. compute a triangulation $\mathcal{T}$ of P
2. Initialize a stack containing all the edges of $\mathcal{T}$
3. **While** stack is non-empty
4. **do** pop ab from stack and unmark it
5. **if** ab is illegal **then**
6. **do** flip ab to cd
7. **for** $xy \in \{ac, cb, bd, da\}$
8. **do if** xy is not marked
9. **then** mark xy and **push** it on stack
10. **return** $\mathcal{T}$

2.2.3. Vertebrae Pose Localization

In this stage, the preceding step's mesh structure is utilized to govern the vertebrae posture area. As observed in Figure 8a, the region of the vertebral poses acquires more of a mesh edge than the region between the poses, as shown in Figure 8b.

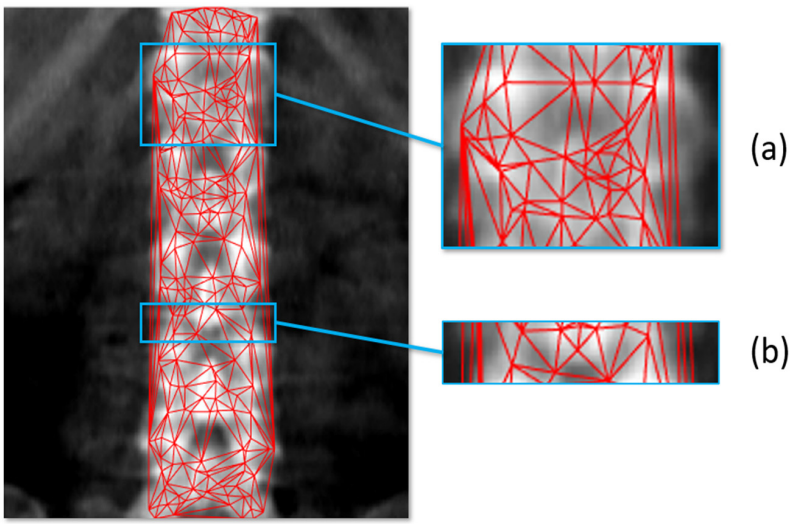

Figure 8. (**a**) Delaunay triangulation structure of vertebrae pose area and (**b**) the gap between pose.

Therefore, the area of the vertebrae can be determined by adjusting the number of edges connecting to each node. It is mean that the area is coarsely located using the faces of the Delaunay triangles. The method is detailed in Algorithm 2.

Algorithm 2 Delaunay's edge counting algorithm

Algorithm Delaunay Edge Counting
input directed graph (DT) $G = (V, E)$ with edge lengths $\lambda : E \to \mathbb{R}_{>0}$
data priority queue Q with keys dist$[\cdot]$, number of edge v

initialization
while Q *not empty* do
  extract $v \leftarrow Q$ with minimum dist$[v]$; push $v \to S$
  foreach vertex w such that $(v, w) \in E$ do
    path discovery //-shorter path to w?
      if dist$[w] >$ dist$[v] + \lambda(v, w)$ then
        dist$[w] \leftarrow$ dist$[v] + \lambda(v, w)$
        Insert/update $w \to Q$ with new key; $\sigma[w] \leftarrow 0$;
        Pred$[w] \leftarrow$ empty list
    path counting
      if dist$[w] =$ dist$[v] + \lambda(v, w)$ then
        $\sigma[w] \leftarrow \sigma[w] + \sigma[v]$
        append $v \to$ Pred$[w]$

Finally, each area of the lumbar L1–L4 vertebrae of the anterior–posterior (AP) and lateral (LA) is located and registered using its density. The triangulation of both views is shown in Figure 9.

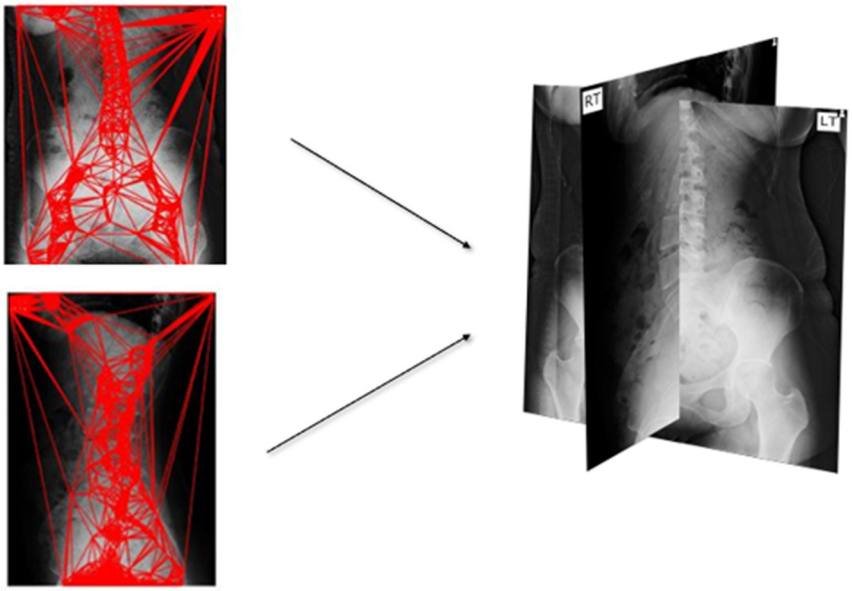

Figure 9. Triangulation of AP view (**left**) and LA view (**right**).

3. Results and Discussion

Fifty radiographs of the human lateral spine were used to compile the data set for the laboratory experiment. We evaluated the performance using the BUU-LSPINE dataset which was collected from Burapha University between February 2021 and November 2022. The dataset contains photos of a good quality, medium quality, and bad quality. These differences are a result of the varied radiation dosages received by each patient. The more radiation that is used to form an image, the higher the quality of the resulting image. During the experiment, both the ground-truth photographs and the automatic lumbar segmentation were assessed. The precision and recall are the two performance criteria that

are measured (the confusion matrix). According to the results of the test which shows in Table 2, the suggested technique enhanced the accuracy by 80.32 percent, the precision by 90 percent, and the recall by 88.5 percent.

Table 2. Experimental result using confusion matrix.

Dataset	Confusion Matrix			
	Accuracy	Recall	Precision	FNR
Good	87.60	88.32	84.24	11.56
Medium	81.38	86.55	83.11	16.20
Low	71.97	81.23	79.73	18.51
Average	**80.32**	**85.37**	**82.36**	**15.42**

Furthermore, the proposed approach was evaluated using the gold-standard matric, consisting of the Jaccard index measurement (JM), Hausdorff distance (HD), and percentage area difference (PAD). The experimental result shows (Table 3) that the proposed approach reaches the best performance in the evaluation compared with the traditional measurements.

Table 3. Localization result comparation.

Method	Evaluation		
	JM	HD	PAD
Proposed approach	**0.82**	**10.87**	**2.33**
Watershed	0.54	46.28	5.19
DRLSE	0.77	27.98	4.63
Region growing	0.81	32.89	4.48

Moreover, we, therefore, evaluate the proposed approach with the time usages of each of the state-of-the-art methods. The result show that the average time of the proposed method reaches 1.23 s, which is more instantaneous than the other. The result can be demonstrated in Table 4.

Table 4. Performance evaluation.

Method	Average Time Usages (s)			
	Good	Medium	Low	Average time
Proposed approach	0.92	1.04	1.36	1.11
Watershed	1.33	1.89	1.92	1.71
DRLSE	1.74	1.79	1.81	1.78
Region growing	1.56	1.88	2.21	1.88

4. Conclusions

In this study, a technique employing Delaunay triangulation for the lumbar vertebrae localization from the low-radiation radiography images generated by dual-energy X-ray absorptiometry is proposed. The proposed algorithm involves three primary steps. Initially, the grayscale input lumbar image was projected vertically using its vertical pattern for automatic cropping. Using its SURF features as triangle nodes, Delaunay triangulation was then carried out. The posture area of the vertebrae was estimated using the edge density of each node. The proposed approach can automatically identify the human lumbar spine region. This can lessen the radiologists' workload. In general, the proposed method can

be employed as a preliminary step in the bone structure's identification and segmentation in the study. Moreover, the proposed method can be used in the registration step three-dimensional reconstruction and deformation. The segmentation of the lumbar region for particular cases of exostosis and bone collapse will be attempted in future research.

Author Contributions: Conceptualization, W.Y. and K.C.; methodology, W.Y., S.L., S.-H.L., J.-S.J., D.L. and K.C.; software, W.Y.; validation W.Y., S.L., S.-H.L., J.-S.J., D.L. and K.C.; formal analysis, W.Y., J.-S.J., D.L. and K.C.; investigation, W.Y., S.L. and K.C.; resources, W.Y. and S.L.; data curation, W.Y. and S.L.; writing—original draft preparation, W.Y.; writing—review and editing W.Y., S.L., S.-H.L., J.-S.J., D.L. and K.C.; visualization, W.Y. and K.C.; supervision, K.C.; project administration, S.-H.L., J.-S.J. and K.C.; funding acquisition, S.-H.L., J.-S.J. and K.C.; All authors have read and agreed to the published version of the manuscript.

Funding: This research was supported by the Korea Institute of Oriental Medicine (grant number: KSN2022130), South Korea, Research Grant of Burapha University through the National Research Council of Thailand (NRCT), fiscal year 2018, (grant number 2561A1080227), and Faculty of Informatics, Burapha University.

Data Availability Statement: https://services.informatics.buu.ac.th/spine/ (accessed on 21 December 2022).

Acknowledgments: The authors are very grateful and wish to extend their sincere thanks to Athita Onuean and the members of Knowledge and Smart Technology (KST) for their contribution.

Conflicts of Interest: The authors declare no conflict of interest.

References

1. Beutel, J.; Kundel, H.L.; Kim, Y.; Van Metter, R.L.; Horii, S.C. Handbook of medical imaging (volume 3). In *A Treatise on Electricity and Magnetism*, 3rd ed.; Clarendon: Oxford, UK, 1892; Volume 2, pp. 68–73.
2. Horng, M.-H.; Kuok, C.-P.; Fu, M.-J.; Lin, C.-J.; Sun, Y.-N. Cobb Angle Measurement of Spine from X-ray Images Using Convolutional Neural Network. *Comput. Math. Methods Med.* **2019**, *2019*, 6357171. [CrossRef] [PubMed]
3. Gaál, G.; Maga, B.; Lukács, A. Attention u-net based adversarial architectures for chest X-ray lung segmentation. *arXiv* **2020**, arXiv:2003.10304.
4. Vidal, P.L.; de Moura, J.; Novo, J.; Ortega, M. Multi-stage transfer learning for lung segmentation using portable X-ray devices for patients with COVID-19. *Expert Syst. Appl.* **2021**, *173*, 114677. [CrossRef] [PubMed]
5. Zhuang, B.; Rohling, R.; Abolmaesumi, P. Region-of-Interest-Based Closed-Loop Beamforming for Spinal Ultrasound Imaging. *IEEE Trans. Ultrason. Ferroelectr. Freq. Control.* **2019**, *66*, 1266–1280. [CrossRef] [PubMed]
6. Buerger, C.; von Berg, J.; Franz, A.; Klinder, T.; Lorenz, C.; Lenga, M. Combining deep learning and model-based segmentation for labeled spine CT segmentation. *Med. Imaging* **2020**, *11313*, 307–314. [CrossRef]
7. Rak, M.; Steffen, J.; Meyer, A.; Hansen, C.; Tönnies, K. Combining convolutional neural networks and star convex cuts for fast whole spine vertebra segmentation in MRI. *Comput. Methods Programs Biomed.* **2019**, *177*, 47–56. [CrossRef]
8. Shirly, S.; Ramesh, K. Review on 2D and 3D MRI Image Segmentation Techniques. *Curr. Med Imaging* **2019**, *15*, 150–160. [CrossRef]
9. Natalia, F.; Meidia, H.; Afriliana, N.; Al-Kafri, A.S.; Sudirman, S.; Simpson, A.; Bashtawi, M. Development of ground truth data for automatic lumbar spine MRI image segmentation. In Proceedings of the 2018 IEEE 20th International Conference on High Performance Computing and Communications; IEEE 16th International Conference on Smart City; IEEE 4th International Conference on Data Science and Systems (HPCC/SmartCity/DSS), Exeter, UK, 28–30 June 2018; pp. 1449–1454. [CrossRef]
10. Ebrahimzadeh, E.; Fayaz, F.; Ahmadi, F.; Nikravan, M. A machine learning-based method in order to diagnose lumbar disc herniation disease by MR image processing. *MedLife Open Access* **2018**, *1*, 1.
11. Vania, M.; Mureja, D.; Lee, D. Automatic spine segmentation from CT images using Convolutional Neural Network via redundant generation of class labels. *J. Comput. Des. Eng.* **2019**, *6*, 224–232. [CrossRef]
12. Li, Y.; Liang, W.; Zhang, Y.; Tan, J. Automatic Global Level Set Approach for Lumbar Vertebrae CT Image Segmentation. *BioMed Res. Int.* **2018**, 6319879. [CrossRef]
13. Zhou, W.; Lin, L.; Ge, G. *N*-Net: 3D Fully Convolution Network-Based Vertebrae Segmentation from CT Spinal Images. *Int. J. Pattern Recognit. Artif. Intell.* **2019**, *33*, 1957003. [CrossRef]
14. Yang, X.; Lei, Y.; Liu, Y.; Tian, S.; Higgins, K.; Beitler, J.J.; Yu, D.S.; Jiang, X.; Liu, T.; Curran, W.J.; et al. Automatic multi-organ segmentation in thorax CT images using U-Net-GAN. *Med. Phys.* **2019**, *10950*, 1095010. [CrossRef]
15. Gabriel, A.T.; Quaresma, C.; Secca, M.F.; Vieira, P. Development and clinical application of Vertebral Metrics: Using a stereo vision system to assess the spine. *Med Biol. Eng. Comput.* **2018**, *56*, 1435–1446. [CrossRef] [PubMed]
16. Gabriel, A.; Quaresma, C.; Secca, M.; Vieira, P. Vertebral Metrics. In Proceedings of the International Joint Conference on Biomedical Engineering Systems and Technologies, Setubal, Portugal, 12–15 January 2016; pp. 235–240. [CrossRef]

17. Lingayat, N.S.; Tarambale, M.R. A Computer Based Feature Extraction of Lung Nodule in Chest X-Ray Image. *Int. J. Biosci. Biochem. Bioinform.* **2013**, *3*, 624–629. [CrossRef]
18. Nash, C.L.; Moe, J.H. A Study of Vertebral Rotation. *J. Bone Jt. Surg.* **1969**, *51*, 223–229. [CrossRef]
19. Hemalatha, R.; Thamizhvani, T.; Dhivya, A.J.A.; Joseph, J.E.; Babu, B.; Chandrasekaran, R. Active Contour Based Segmentation Techniques for Medical Image Analysis. *Med. Biol. Image Anal.* **2018**, *4*, 2. [CrossRef]
20. Löffler, M.T.; Sekuboyina, A.; Jacob, A.; Grau, A.-L.; Scharr, A.; El Husseini, M.; Kallweit, M.; Zimmer, C.; Baum, T.; Kirschke, J.S. A Vertebral Segmentation Dataset with Fracture Grading. *Radiol. Artif. Intell.* **2020**, *2*, e190138. [CrossRef]
21. Shen, H.; Huang, J.; Zheng, Q.; Zhu, Z.; Lv, X.; Liu, Y.; Wang, Y. A Deep-Learning–Based, Fully Automated Program to Segment and Quantify Major Spinal Components on Axial Lumbar Spine Magnetic Resonance Images. *Phys. Ther.* **2021**, *101*, pzab041. [CrossRef]
22. Kijowski, R.; Liu, F.; Caliva, F.; Pedoia, V. Deep Learning for Lesion Detection, Progression, and Prediction of Musculoskeletal Disease. *J. Magn. Reson. Imaging* **2019**, *52*, 1607–1619. [CrossRef]
23. Grob, A.; Loibl, M.; Jamaludin, A.; Winklhofer, S.; Fairbank, J.C.T.; Fekete, T.; Porchet, F.; Mannion, A.F. External validation of the deep learning system "SpineNet" for grading radiological features of degeneration on MRIs of the lumbar spine. *Eur. Spine J.* **2020**, *31*, 2137–2148. [CrossRef]
24. Goedmakers, C.M.W.; Lak, A.M.; Duey, A.H.; Senko, A.W.; Arnaout, O.; Groff, M.W.; Smith, T.R.; Vleggeert-Lankamp, C.L.A.; Zaidi, H.A.; Rana, A.; et al. Deep Learning for Adjacent Segment Disease at Preoperative MRI for Cervical Radiculopathy. *Radiology* **2021**, *301*, 664–671. [CrossRef] [PubMed]
25. Mbarki, W.; Bouchouicha, M.; Frizzi, S.; Tshibasu, F.; Ben Farhat, L.; Sayadi, M. Lumbar spine discs classification based on deep convolutional neural networks using axial view MRI. *Interdiscip. Neurosurg.* **2020**, *22*, 100837. [CrossRef]
26. Ghosh, S.; Malgireddy, M.R.; Chaudhary, V.; Dhillon, G. A new approach to automatic disc localization in clinical lumbar MRI: Combining machine learning with heuristics. In Proceedings of the 2012 9th IEEE International Symposium on Biomedical Imaging (ISBI), Barcelona, Spain, 2–5 May 2012; pp. 114–117. [CrossRef]
27. Azevedo, T.C.S.; Tavares, J.M.R.S.; Vaz, M.A.P. *3D Object Reconstruction from Uncalibrated Images Using an off-the-Shelf Camera*; Springer: Berlin/Heidelberg, Germany, 2009; pp. 117–136. [CrossRef]
28. Azevedo, T.C.; Tavares, J.M.R.; Vaz, M.A. 3D reconstruction and characterization of human external shapes from 2D images using volumetric methods 3D reconstruction and characterization of human external shapes from 2D images using volumetric methods. *Comput. Methods Biomech. Biomed. Eng.* **2010**, *13*, 359–369. [CrossRef] [PubMed]
29. Zhao, Y.J.; Shi, L.; Li, J.; Griffith, J.F.; Ahuja, A.T.; Heng, P. Vertebra segmentation of spine MRI with improved GVF snake based on shape knowledge. In Proceedings of the 2011 International Conference on Machine Learning and Cybernetics, Guangxi, China, 10–13 July 2011; Volume 4, pp. 1867–1871.
30. Pintar, F.A.; Yoganandan, N.; Myers, T.; Elhagediab, A.; Sances, A., Jr. Biomechanical properties of human lumbar spine ligaments. *J. Biomech.* **1992**, *25*, 1351–1356. [CrossRef] [PubMed]
31. Rahman, M.; Cao, Y.; Sun, X.; Li, B.; Hao, Y. Deep pre-trained networks as a feature extractor with XGBoost to detect tuberculosis from chest X-ray. *Comput. Electr. Eng.* **2021**, *93*, 107252. [CrossRef]